## **OPEN ACCESS**



# **Hydrohalite Salt-albedo Feedback Could Cool M-dwarf Planets**

Aomawa L. Shields<sup>1</sup> and Regina C. Carns<sup>2</sup>

Department of Physics and Astronomy, University of California, Irvine, 4129 Frederick Reines Hall, Irvine, CA 92697-4575, USA; shields@uci.edu
Polar Science Center Applied Physics Laboratory, University of Washington, Seattle, WA 98105-6698, USA
Received 2018 March 21; revised 2018 August 7; accepted 2018 August 21; published 2018 October 25

#### **Abstract**

A possible surface type that may form in the environments of M-dwarf planets is sodium chloride dihydrate, or "hydrohalite" (NaCl · 2H<sub>2</sub>O), which can precipitate in bare sea ice at low temperatures. Unlike salt-free water ice, hydrohalite is highly reflective in the near-infrared, where M-dwarf stars emit strongly, making the effect of the interaction between hydrohalite and the M-dwarf spectral energy distribution necessary to quantify. We carried out the first exploration of the climatic effect of hydrohalite-induced salt-albedo feedback on extrasolar planets, using a three-dimensional global climate model. Under fixed CO<sub>2</sub> conditions, rapidly rotating habitable-zone M-dwarf planets receiving 65% or less of the modern solar constant from their host stars exhibit cooler temperatures when an albedo parameterization for hydrohalite is included in climate simulations, compared to simulations without such a parameterization. Differences in global mean surface temperature with and without this parameterization increase as the instellation is lowered, which may increase CO<sub>2</sub> build-up requirements for habitable conditions on planets with active carbon cycles. Synchronously rotating habitable-zone M-dwarf planets appear susceptible to salt-albedo feedback at higher levels of instellation (90% or less of the modern solar constant) than planets with Earth-like rotation periods, due to their cooler minimum dayside temperatures. These instellation levels where hydrohalite seems most relevant correspond to several recently discovered potentially habitable M-dwarf planets, including Proxima Centauri b, TRAPPIST-1e, and LHS 1140b, making an albedo parameterization for hydrohalite of immediate importance in future climate simulations.

Key words: astrobiology – planetary systems – radiative transfer – stars: low-mass

#### 1. Introduction

Planetary climate and habitability are strongly affected by the interaction between the spectral energy distribution (SED) of the planet's host star and the planet's unique surface composition. Surface types exhibit wavelength-dependent radiative properties, making their interactions with different host star SEDs distinct and challenging to model. This complexity is particularly acute for planets orbiting M-dwarf stars, whose near-infrared (near-IR) emission coincides with clear differences in the albedo of specific surface types such as ocean, water ice, and snow at these wavelengths (Joshi & Haberle 2012; Shields et al. 2013, 2014, 2016a).

Here, we consider the radiative properties and impact on habitability (the capability of sustaining liquid water on some part of a planet's surface; e.g., Seager 2013) of a surface type never before considered in the context of extrasolar planets—sodium chloride dihydrate, or "hydrohalite" (NaCl  $\cdot$  2H<sub>2</sub>O). At low temperatures ( $T < -23^{\circ}$ C) on planets with oceans, salt within brine inclusions in bare sea ice can precipitate in crystal form, eventually forming a hydrohalite crust (Carns et al. 2016; Light et al. 2016). As shown in Figure 1, hydrohalite is much more reflective than bare sea ice in the near-IR, resulting in higher broadband albedos than even snow. The net impact of the surface salt-albedo feedback mechanism generated by hydrohalite formation on extrasolar planets has not previously been explored.

Studies of hydrohalite crusts have been applied to episodes of global-scale glaciation during the Neoproterozoic periods

Original content from this work may be used under the terms of the Creative Commons Attribution 3.0 licence. Any further distribution of this work must maintain attribution to the author(s) and the title of the work, journal citation and DOI.

(600–800 million years ago) on Earth (Light et al. 2009, 2016; Carns et al. 2016), the so-called "Snowball Earth" events (Kirschvink 1992). Low surface temperatures (<30°C) in the tropics during Snowball Earth events (Pierrehumbert 2005) may have inhibited melting for long enough for hydrohalite crusts to form over wide areas (Light et al. 2009). In regions of net sublimation in the tropics, where low-latitude ice was present and receiving the majority of the solar insolation, climate would have been far more sensitive to sea ice albedo than in higher-latitude ice-covered regions (Light et al. 2009). The high visible and near-IR albedos of hydrohalite crusts, compared with the salt-free ice albedos previously used in climate modeling of low-latitude glacial episodes, could have significantly altered the surface energy balance of Snowball Earth (Carns et al. 2016).

M-dwarf stars are the most common type of stars in the galaxy, and discovering habitable planets around these stars will be the focus of extrasolar planet observational efforts for the foreseeable future, by both large-aperture (30 m class) telescopes on the ground, and space-based observatories such as the *Transiting Exoplanet Survey Satellite* (Ricker et al. 2014). Identifying those potentially habitable planets to target for follow-up by the *James Webb Space Telescope* (Gardner et al. 2006; Kalirai 2018) and the next generation of space missions depends on understanding the impact on habitability of the different interactions between the M-dwarf SED and specific surface types that may be possible on M-dwarf planets, as these interactions defy existing modeling prescriptions.

Near the outer edge of the habitable zone, where a number of potentially habitable M-dwarf planets have been discovered (Quintana et al. 2014; Dittmann et al. 2017; Gillon et al. 2017), surface temperatures on regions of a planet may reach well below  $-23^{\circ}$ C (depending on atmospheric greenhouse gas

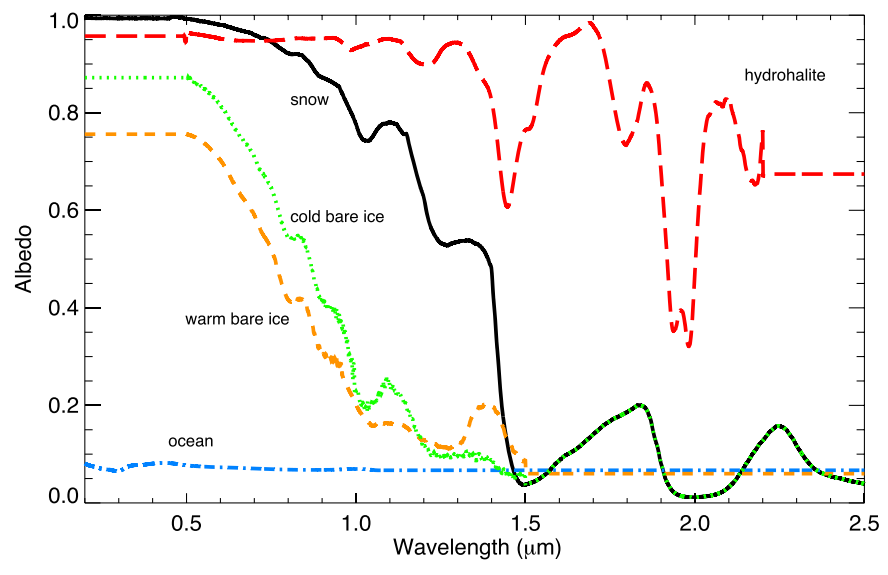


Figure 1. Spectral distribution of sodium chloride dihydrate, or "hydrohalite" (NaCl · 2H<sub>2</sub>O) from Light et al. (2016), fine-grained snow (H<sub>2</sub>O, free of salts; Hudson et al. 2006), cold and warm bare ice (Light et al. 2016), and ocean (from Brandt et al. 2005).

Table 1
Two-band Albedos Employed for Different Temperature Regimes (Given in Degrees Celsius) Reached in the GCM, Weighted by the Spectrum for G-dwarf Star the Sun and M-dwarf Star AD Leo

Host Star	$0^{\circ} > T > -23^{\circ}$	$-23^{\circ} > T > -40^{\circ}$	$T < -40^{\circ}$	E-P<0
Band	NIR/VIS	NIR/VIS	NIR/VIS	NIR/VIS
M-dwarf	0.18/0.69	0.21/0.80	0.88/0.95	0.49/0.97
G-dwarf	0.30/0.67	0.31/0.84	0.90/0.96	0.68/0.80

Note. For temperatures below  $-23^{\circ}$ C, the albedos given incorporate our hydrohalite parameterization applied to the model. E and P denote water evaporation and precipitation, respectively.

concentrations), where hydrohalite formation may occur, making the climatic effect of this possible surface type on M-dwarf planets particularly important to quantify.

In this work, we calculate the effect of hydrohalite-induced salt-albedo feedback on the climate of ocean-covered planets orbiting M-dwarf stars and compare these results to those for similar planets modeled without a parameterization for hydrohalite formation. We identify climate regimes where this surface type could be most relevant and impactful for the surface habitability of M-dwarf planets with Earth-like atmospheres and discuss differences in the climatic effect of this surface type for planets orbiting brighter, Sun-like stars.

In Section 2, we present and explain our methods and models used. In Sections 3 and 4, we present and discuss the results and significance of our simulations. In Section 5, we offer concluding remarks and implications of this work for future studies of the potential climates of recently discovered potentially habitable exoplanets.

## 2. Methods and Models

We used the Community Climate System Model (CCSM), a three-dimensional (3D) global climate model (GCM) developed to simulate past and present climate states on Earth (Gent et al. 2011). With an atmospheric component (Community Atmosphere Model version 4, or CAM4), the Los Alamos sea ice model (CICE version 4; Hunke & Lipscomb 2008), and a 50 m deep, slab ocean, we refer collectively to this suite of coupled model components as CCSM4, as done in previous work (see,

e.g., Bitz et al. 2012; Shields et al. 2013, 2014, 2016b). The ocean is treated as static, but fully mixed with depth. Simulations that include a fully dynamic ocean are too computationally expensive to permit the exploration of a broad range of forcing parameters as we do in this work. The horizontal angular resolution is 2°. We simulated the climates of M- and G-dwarf aquaplanets (no land), with circular orbits; Earth's radius, mass, and obliquity; atmospheres with 1-bar surface pressure; and Earth-like levels of CO<sub>2</sub>. We simulated both Earth-like (24 hr) and synchronous rotation periods. Atmospheric water vapor was allowed to vary during each simulation according to evaporation and precipitation processes on the surface and in the atmosphere.

The sea-ice albedo parameterization in CCSM3, as used in Shields et al. (2013, 2014, 2016b), divides the surface albedo into two bands, visible ( $\lambda \leq 0.7~\mu m$ ) and near-IR ( $\lambda > 0.7~\mu m$ ), because it is easier to control than the multiple-scattering scheme in later code versions. The default near-IR and visible band albedos are 0.3 and 0.67 for cold bare ice, and 0.68 and 0.8 for cold dry snow, respectively. We used these default values for our G-dwarf planet climate simulations, as they are tuned for an incident solar spectrum and yield modern-day Earth climates for simulations of planets receiving 100% of the modern solar constant. However, for our simulations of M-dwarf planet climates, we calculated the two-band albedos weighted by the specific spectrum of our M-dwarf host star and used those values (Table 1) for greater accuracy.

Modifications were made to the ice thermal code in CICE4, based on the original model written by Bitz et al. (2001), to

incorporate the bare sea-ice albedo change due to crystallization of hydrohalite at low temperatures, and the subsequent formation of a hydrohalite crust. In the model, sea ice is allowed to form as surface temperatures reach the freezing point of liquid water. Areas of net water precipitation were assigned two-band albedos for salt-free snow with  $100\,\mu\mathrm{m}$  sized grains. For temperatures between freezing and the temperature where hydrohalite begins to precipitate in sea ice ( $T < -23\,^{\circ}\mathrm{C}$ ), we used two-band albedos for salt-free, "warm" bare ice; below  $-23\,^{\circ}\mathrm{C}$ , we used two-band albedos for cold bare ice with precipitated hydrohalite; and below  $-40\,^{\circ}\mathrm{C}$ , we used two-band albedos for a fully formed hydrohalite crust. Two-band albedos weighted by the spectrum of each host star and used for each temperature regime are given in Table 1.

To allow for the simulation of planets orbiting stars with different SEDs, the percentages of incoming stellar flux in each of the 12 wavelength bands that are input to CAM4 were varied according to the SED of the host star (see, e.g., Shields et al. 2013, 2014, 2016b). We employed the solar spectrum obtained from Chance & Kurucz (2010) and a spectrum for M3V star AD Leo (Reid et al. 1995; Segura et al. 2005) obtained from the Virtual Planetary Laboratory. Flux from the M-dwarf star outside of the CAM4 wavebands for shortwave (incoming) flux was folded into the shortest and longest wavebands so that the entire stellar spectrum was incorporated, as done in prior work (Shields et al. 2013, 2014).

Although the crystallization of hydrohalite has been shown to start once temperatures reach  $-23^{\circ}\text{C}$  (Carns et al. 2015), the formation of a hydrohalite crust depends on temperatures staying below this value throughout a diurnal cycle. It is possible that temperatures could rise to a level sufficient for melting of a hydrohalite crust during the simulation. The albedo of a dissolving hydrohalite crust is significantly reduced at all wavelengths compared with fully formed hydrohalite (Carns et al. 2016). Abbot et al. (2010) identified a diurnal temperature variation in glaciated regions of  $\sim \pm 10^{\circ}$ . We therefore used  $-40^{\circ}\text{C}$  as the surface temperature requirement for hydrohalite crust formation to provide a conservative 17° buffer that increased the likelihood that temperatures remained cold enough for application of the hydrohalite crust albedos.

The climatic effects of a hydrohalite crust are governed by the exposure of an icy planetary surface to incident stellar radiation, and therefore depend on water evaporation exceeding precipitation (E-P>0) in the surrounding ice. Where E-P<0, it can be expected that snow will cover the planetary surface in that particular location, masking any albedo differences between the different parameterizations in our model. We discuss the effect of regions of net water precipitation on the climatic impact of hydrohalite formation in later sections.

We ran GCM simulations in which we included the hydrohalite parameterization described above ("HH"), as well as with the default ice albedo parameterization, where bare seaice near-IR and visible albedos remain fixed at salt-free values for all surface temperatures below freezing ("Control"). We simulated a range of levels of incident stellar insolation ("instellation") and focus our study here on instellation levels that bracket important climate regimes at fixed, Earth-like levels of CO<sub>2</sub> (400 ppmv).

First, we explore the degree of influence on climate of applying the albedo effects of hydrohalite crust formation in simulations of planets receiving the requisite amount of instellation to yield global mean surface temperatures similar to modern-day Earth. We then compare our results with those for climates where a narrow region of open water is present in the tropics—so called "waterbelt" states (Wolf et al. 2017). Finally, we examine simulations of M-dwarf planets in fully glaciated, "snowball" states (Kirschvink 1992). Given that M-dwarf habitable-zone planets may (Dole 1964; Kasting et al. 1993; Joshi et al. 1997; Edson et al. 2011) or may not (Leconte et al. 2015) be synchronously rotating, we simulate planets with both 24 hr and synchronous rotation periods to bracket the possible effects of rotation period on climate sensitivity to salt-albedo feedback. We also compare the climatic impact of the salt-albedo feedback mechanism induced by hydrohalite formation on M-dwarf planets with that on G-dwarf planets, using select simulation runs of G-dwarf aquaplanets at similar instellation values. We present our results and comparison in the following section.

## 3. Results

Figure 2 shows annually averaged values as a function of latitude for surface temperature, ice cover fraction, surface albedo, and water evaporation minus precipitation (E-P), for an M-dwarf planet with a 24 hr rotation period receiving 90% of the modern solar constant from its host star. It includes both the Control case, without hydrohalite albedos assigned for relevant temperatures, and the HH case, with the temperature-dependent hydrohalite albedo parameterization included. The global mean surface temperature is  $\sim$ 290 K, slightly warmer than modern-day Earth (288 K).

As shown in Figure 2(a), surface temperatures do not reach below ~258 K anywhere on the planet in either parameterization at this instellation. The hydrohalite parameterization, which is set in our model to apply higher bare ice albedos when temperatures reach  $-23^{\circ}$ C (250 K), is therefore not relevant in this regime, resulting in equivalent patterns of E - P on both planets (Figure 2(b)), and similar surface albedos (Figure 2(c)). The regions of net evaporation between  $0^{\circ}$  and  $\sim 40^{\circ}$ S and  $0^{\circ}$  and  $\sim 40^{\circ} N$  occur where there is no ice present to be exposed to incoming stellar radiation (Figure 2(d)). We confirm similar results in our simulation of a G-dwarf aquaplanet receiving 100% of the modern solar constant, whose surface climate has been shown in previous work to be analogous to that of an M-dwarf aquaplanet at 90% instellation, due to increased IR absorption by surface water ice and snow, as well as atmospheric CO<sub>2</sub> and water vapor (Shields et al. 2013). Differences in surface temperature and ice fraction are minimal (Figures 2(e) and (f)).

Figure 3 shows similar calculated values for the M-dwarf planet receiving 65% instellation from its host star for both the HH and Control cases. Our simulations showed this instellation to be the lowest received by the planet without becoming fully glaciated. Here, we see that minimum surface temperatures reached  $\sim\!202\,\mathrm{K}$  in both simulations (Figure 3(a)). There are still largely similar regions of net water precipitation between the two planets everywhere except in the equatorial regions. Here, the water precipitation rate drops slightly at the equator in the HH case compared to the Control case (Figure 3(b)), due to lower amounts of cloud cover on the planet with the hydrohalite parameterization, weaker Hadley circulation, and

<sup>3</sup> http://vpl.astro.washington.edu/spectra/stellar/mstar.htm

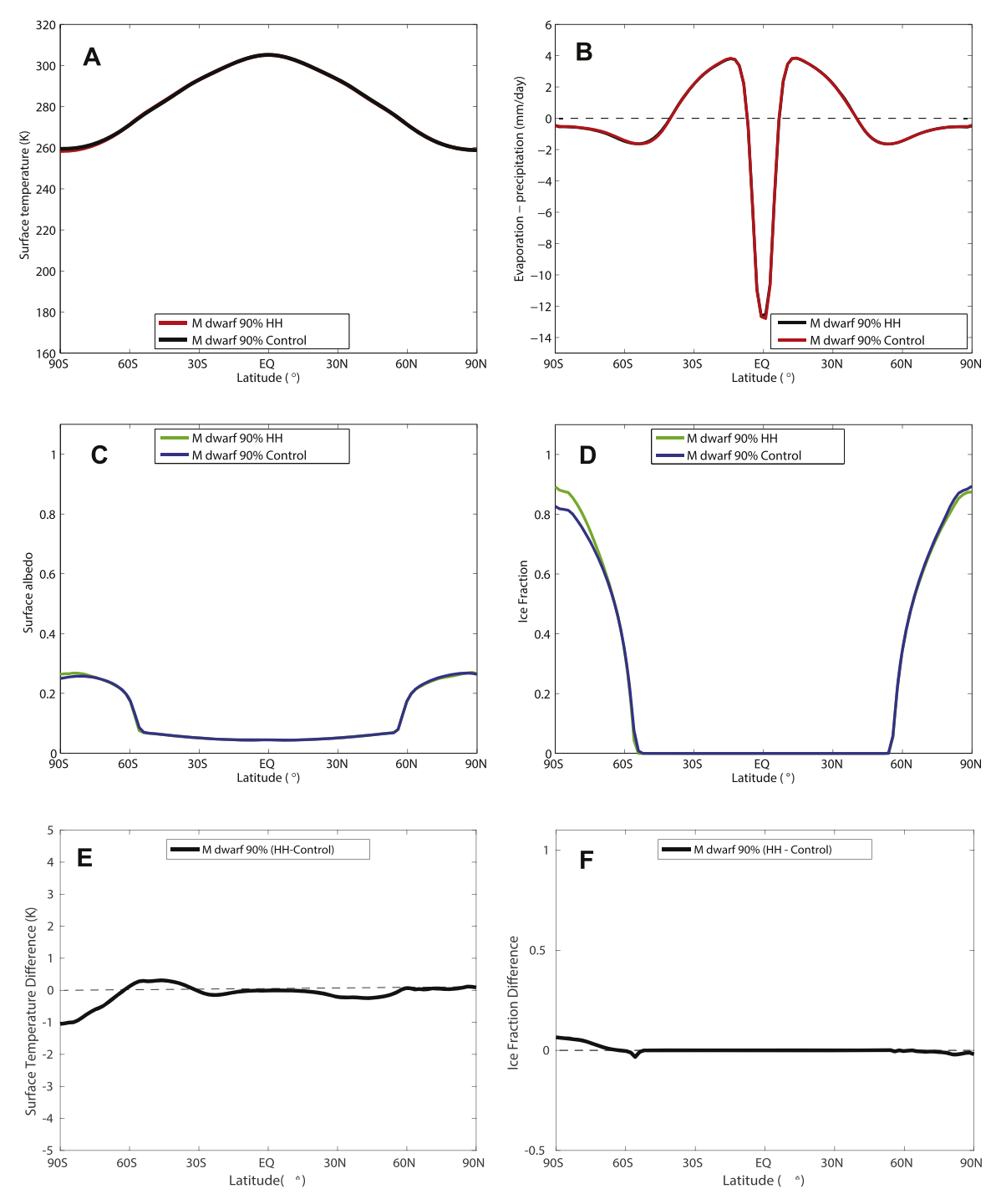


Figure 2. Annually averaged surface temperature (top left), water evaporation minus precipitation (top right), surface albedo (middle left), ice fraction (middle right), surface temperature difference (bottom left), and ice fraction difference (bottom right) as a function of latitude for an M-dwarf planet with a 24 hr rotation period receiving 90% of the modern solar constant from its star after 80 year CCSM4 GCM simulations.

more shortwave radiation absorbed by the surface at the equator compared to the Control case. Surface albedos (Figure 3(c)) are slightly higher in the HH case, and global mean surface temperatures begin to differ slightly between the HH and Control cases, at  $\sim\!249\,\mathrm{K}$  and  $\sim\!251\,\mathrm{K}$ , respectively, though both planets still have similarly narrow swaths of open water at the equator (Figure 3(d)). Differences in surface temperature are larger at this instellation (Figure 2(e)), particularly where albedo differences are larger between the

HH and Control cases in the mid- to upper latitudes. The ice fraction difference also coincides with net positive E - P.

As M-dwarf planets orbiting in their host stars' habitable zones may be synchronously rotating (Kasting et al. 1993; Shields et al. 2016a), we also ran select simulations of planets in such an orbital configuration, with our planets at zero eccentricity and an obliquity of 23°. Figure 4 shows surface temperatures on synchronously rotating M-dwarf planets at 90% and 65% instellation in the Control case (no hydrohalite

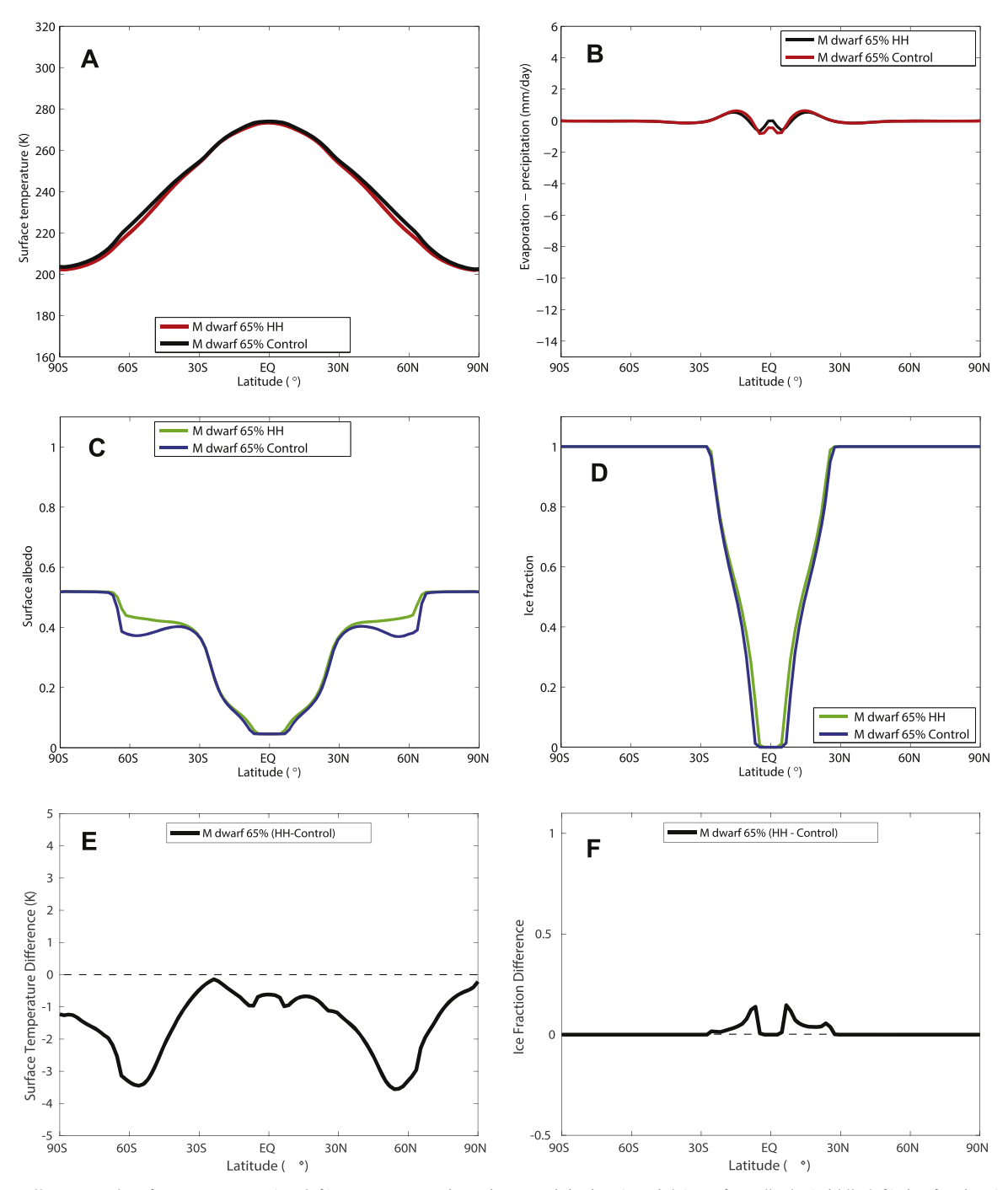


Figure 3. Annually averaged surface temperature (top left), water evaporation minus precipitation (top right), surface albedo (middle left), ice fraction (middle right), surface temperature difference (bottom left), and ice fraction difference (bottom right) as a function of latitude for an M-dwarf planet receiving 65% of the modern solar constant from its star after 80 year CCSM4 GCM simulations.

albedo parameterization), along with ice cover fraction for synchronously rotating M-dwarf planets at 65% planets in the HH and Control cases. Also shown are E-P and latitudinal change in surface temperature at a range of instellations for planets with Earth-like rotation periods orbiting M- and G-dwarf stars. While the difference between the Control and HH cases is negligible at 90% instellation for our simulated M-dwarf planets with Earth's rotation period (Figure 2), the colder temperatures exhibited on the dayside of the synchronously rotating M-dwarf planets at equivalent instellation

reached  $\sim$ 219 K in the Control case (Figure 4(a))—the regime where hydrohalite could begin to precipitate in sea ice. However, global mean surface temperatures were still approximately equal ( $\sim$ 241 K) in both the Control and HH cases, with similar ice cover fraction.

The difference between the HH and Control simulations is stronger in the synchronous case at 65% instellation, where minimum temperatures reached  $\sim\!\!200\,K$  on the dayside of the planet in the Control case (Figure 4(b)) and  $\sim\!\!197\,K$  in the HH case, leading to global mean surface temperatures that were  $\sim\!\!10\,K$ 

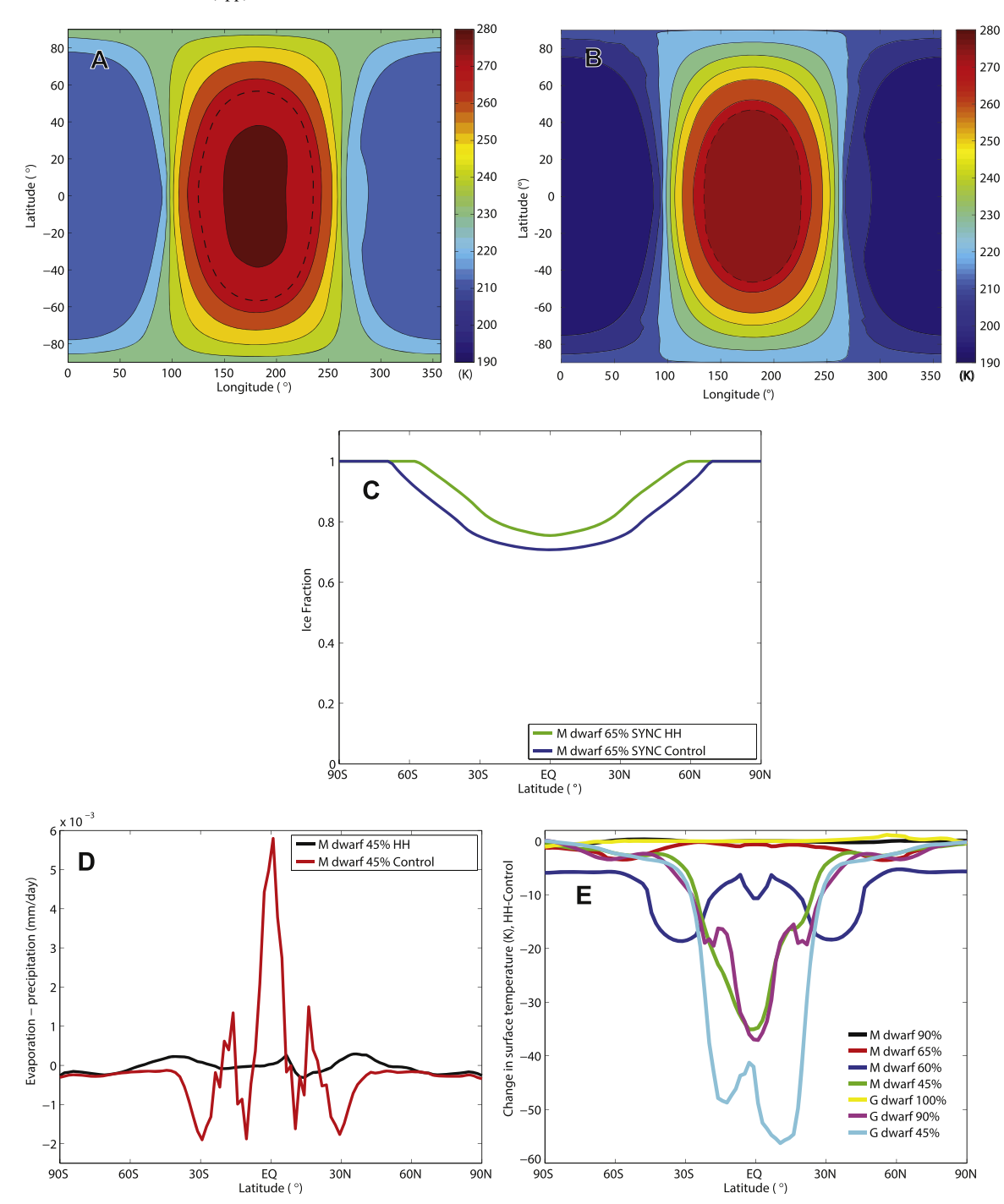


Figure 4. Top: surface temperature as a function of latitude and longitude on synchronously rotating planets receiving 90% (left) and 65% (right) of the modern solar constant from an M-dwarf star (Control case) after 60 and 80 year CCMS4 simulations, respectively. Zero eccentricity and an obliquity of 23° is assumed. The freezing point (273 K) on each planet is labeled by a dashed contour line. Middle: ice fraction as a function of latitude for a synchronously rotating M-dwarf planet receiving 65% of the modern solar constant from its host star. Bottom left: water evaporation minus precipitation as a function of latitude for an M-dwarf planet receiving 45% of the modern solar constant from its star after 80 year CCSM4 simulations. Bottom right: change in surface temperature as a function of latitude on simulated planets with the hydrohalite parameterization (compared to the Control case) and receiving different levels of instellation from M- and G-dwarf stars after 80 model years of simulation.

colder on the planet with the hydrohalite parameterization. This resulted in larger differences in ice cover fraction (Figure 4(c)) between the two synchronously rotating cases at 65% compared to simulations with Earth's rotation period (Figure 3(d)).

The differences between the HH and Control cases become even larger at lower instellation. As shown in Figure 4(d), although the hydrological cycle has lessened significantly on an ice-covered M-dwarf planet receiving 45% of the modern solar

constant from its host star, the larger relative amount of evaporation in the warmer Control case allows for differences in surface albedo to become much more integral to the resulting climate. Furthermore, the lower the instellation received by the planet from the M-dwarf star, the greater the differences in surface temperature across the planet (Figure 4(e)), particularly in the tropics where regions of net evaporation are present. The effect of reduced surface temperatures when a hydrohalite

parameterization is included is even stronger on G-dwarf planets at low values of instellation, given the increased visible and UV output of their host stars, which has been shown to increase climate sensitivity to water-ice-albedo feedback on G-dwarf planets (see, e.g., Shields et al. 2013, 2014).

## 4. Discussion

Our results indicate that when parameterizations are included in 3D climate models to allow for the possible formation of hydrohalite in bare sea ice on extrasolar planets, the climatic effect of the resulting salt-albedo feedback mechanism could be significant at 65% and lower values of instellation within the habitable zone and 90% and lower values of instellation for synchronously rotating M-dwarf planets, assuming fixed  $\rm CO_2$  levels. The large difference in reflectivity between water ice and hydrohalite in the near-IR make this surface type particularly relevant to consider in simulating planets around M-dwarf stars, as they emit strongly in this region of the spectrum. Such planets could be colder at a given instellation than prior calculations would suggest.

For M-dwarf planets with global mean surface temperatures similar to modern-day Earth and rotation periods equal to those of Earth (24 hr), temperatures do not drop low enough for the crystallization of hydrohalite. However, for synchronously rotating M-dwarf planets receiving similar instellation, the low temperatures required for hydrohalite crystallization and crust formation ( $-23^{\circ}$ C and  $-40^{\circ}$ C, respectively) are reached on the dayside of these planets (assuming Earth-like atmospheric levels of CO<sub>2</sub>), even in the middle range of the habitable zone. This may increase the likelihood of snowball states on synchronously rotating planets, although active carbon cycles, if present on these planets, may prevent the occurrence of such states (Checlair et al. 2017).

Orbit precession can cause even those planets affected by tides to retain constant non-zero obliquity, which has been shown to protect a planet from the most severe temperature extremes and improve conditions for surface habitability (Dobrovolskis 2009). Our results with an obliquity of 23° in our simulations of synchronous planets therefore constitute a lower limit on the effects of the hydrohalite parameterization on synchronously rotating habitable-zone planets compared to those with zero obliquity.

Though differences in global mean surface temperatures are still negligible between synchronous HH and Control cases in the middle of the habitable zone, we find larger differences in global mean surface temperature at lower levels of instellation within the habitable zone ( $\leq 65\%$  of the modern solar constant), where there is still open water present on the planet, compared to simulations of planets without our hydrohalite parameterization. Synchronous rotation on simulated aquaplanets has been shown to cause weakened low-latitude zonal winds (Edson et al. 2011) and larger total cloud cover (Yang et al. 2014), which cool the planets compared to planets with faster rotation periods. Hydrohalite may therefore be an important and plausible surface type to form on synchronously rotating habitable-zone M-dwarf planets such as Proxima Centauri b and TRAPPIST-1e, which receive 65% and  $\sim$ 60% of the modern solar constant from their host stars, respectively, and are both expected to be synchronously rotating (Anglada-Escudé et al. 2016; Gillon et al. 2017).

Climatic differences between M-dwarf planets with and without a hydrohalite parameterization included in the model

are especially large for so-called "waterbelt" planets with narrow swaths of open water in the tropics and for planets that are colder, assuming an Earth-like amount of CO<sub>2</sub>. We find that as the instellation is lowered in our simulations, the difference in global mean surface temperature between the planets in the HH and Control cases increases. For our M-dwarf planets receiving 45% instellation, similar to recently discovered planet LHS 1140b (46%; Dittmann et al. 2017), the global mean surface temperature is 12°C colder on the planet with the hydrohalite parameterization. This difference has two important implications. First, planets like LHS 1140b, which is still in the habitable zone of its host star, would likely require more CO<sub>2</sub> to build up in their atmospheres, as the silicate weathering rate decreases (e.g., Walker et al. 1981) than previously expected to keep the planet warm enough for surface liquid water, as these planets could be much colder than originally assumed. Second, frozen planets near or outside the outer edge of their stars' habitable zones, with only the steady brightening of their host stars over time to depend on to eventually generate abovefreezing surface temperatures, would likely have higher instellation thresholds for melting and surface habitability than might otherwise be proposed. Additionally, the resulting cooler climates as a consequence of hydrohalite crystallization may make it more difficult for so-called limit cycles between snowball and warm climates (e.g., Menou 2015; Abbot 2016; Haqq-Misra et al. 2016) to operate on planets with sufficiently low values of instellation or introduce limit cycles previously believed unlikely on M-dwarf planets (Haqq-Misra et al. 2016), as a result of hydrohalite-induced salt-albedo feedback.

Planets orbiting G-dwarf stars exhibited even greater decreases in surface temperature, compared to M-dwarf planets, when the hydrohalite parameterization was included in the simulation. This is due to their increased sensitivity to water-ice-albedo feedback, which contributes significantly to the lower surface temperatures on G-dwarf planets at a given instellation. Our results demonstrate that hydrohalite could have a significant climatic impact on cold, dry G-dwarf planets as well, should they be present at the distant outer regions of their host stars' habitable zones.

Although we used the default two-band visible and near-IR salt-free ice and snow albedos for our climate simulations of G-dwarf planet climates, we employed values weighted by our G-dwarf spectrum from Chance & Kurucz (2010) in our albedo parameterization for hydrohalite crystallization and crust formation. The values for salt-free ice and snow calculated with our outside solar spectrum are higher than the default values employed in the GCM, resulting in even colder temperatures on simulated G-dwarf planets compared to our M-dwarf simulations. We therefore elected to include the G-dwarf simulations that used the default salt-free albedos here, because they yield modern-day Earth-like climates at Earth's current instellation level (100% of the modern solar constant), providing a useful reference point. These simulations therefore constitute a lower limit on the climatic differences possible between G-dwarf planets and M-dwarf planets due to hydrohalite effects.

The climatic effects of hydrohalite presented here depend on the presence of oceans on these planets. Planets composed predominantly of land have been shown to be less susceptible to episodes of global-scale glaciation (Abe et al. 2011), and the small area of sea ice on such planets would limit the effect of salt-albedo feedback. The low potential water inventory on M-dwarf planets, due to low planetary disk mass (Raymond et al. 2007) or ocean evaporation as the result of an extended pre-main-sequence host star phase (Luger & Barnes 2015), could certainly impact the likelihood of hydrohalite formation in sea ice. However, M-dwarf planets subjected to water loss may still retain enough water to maintain habitable surface conditions, depending on their initial water content (e.g., Bolmont et al. 2017). Additionally, our results would naturally be sensitive to ocean salinity, which is unconstrained on exoplanets. On Earth, salinity levels in young sea ice vary from 12 to 20 parts per thousand by mass (%o) from seawater of normal salinity (32%0-35%0). The salt is present in the form of brine inclusions; as the sea ice cools, water freezes onto the walls of the inclusions, concentrating the brine until it reaches the temperature and salinity threshold for salt crystallization (Carns et al. 2015). We have adopted a temperature threshold for hydrohalite crystallization appropriate for the mixture of salts present in Earth seawater. On planets with lower seawater salinity, or where sodium chloride is not the most common salt in seawater, it may be more difficult for hydrohalite to form.

## 5. Conclusions

Using a three-dimensional GCM modified to incorporate an albedo parameterization for sodium chloride dihydrate, or "hydrohalite" (NaCl · 2H<sub>2</sub>O)—a surface type previously unexplored in the context of extrasolar planets—we have shown that simulations that include the salt-albedo feedback mechanism generated by the crystallization of this surface type in bare sea ice result in lower planetary global mean surface temperatures compared to simulations without this parameterization included, assuming Earth-like levels of CO<sub>2</sub>. The large differences between the albedo of hydrohalite and water ice in the near-IR are primarily responsible for the difference in global mean surface temperatures on simulated M-dwarf planets with and without the hydrohalite parameterization included. G-dwarf planets, which exhibit greater climate sensitivity to water-ice-albedo feedback and are therefore cooler to begin with at a given instellation, exhibit even stronger planetary cooling in simulations incorporating the albedo effects of this surface type. The climatic effect of hydrohalite becomes particularly important on rapidly rotating habitable-zone M-dwarf planets receiving 65% instellation from their host stars, with narrow swaths of open water. Habitable-zone M-dwarf planets that are synchronously rotating and receiving less than 90% instellation from their host stars exhibit increased susceptibility to the climatic effects of this surface type, due to colder minimum surface temperatures reached on the dayside of the planet compared with planets with Earth-like rotation periods receiving similar instellation. The effect is even stronger on fully glaciated planets, where net water evaporation exceeds precipitation such that differences in surface albedo are exposed to incoming stellar radiation, rather than masked by falling snow. These planets are therefore likely to be even colder than originally presumed, given the incorporation of an albedo parameterization for hydrohalite formation in climate simulations. The habitable-zone instellation values where the climatic effects of hydrohalite appear most relevant correspond to those of several recently discovered potentially habitable M-dwarf planets, including LHS 1140b, TRAPPIST-1e, and Proxima Centauri b; therefore, future simulations of the potential climates of these planets would benefit from inclusion of the hydrohalite albedo

parameterization that we have developed and incorporated here. By depressing global mean surface temperatures, hydrohalite could increase the greenhouse gas concentration required to maintain surface liquid water on planets near the outer edge of their host stars' habitable zones. It may also increase the instellation values necessary to perpetuate free-thaw cycles on planets with nonzero eccentricities or other sources of climate cycling.

This material is based upon work supported by NASA under grant number NNH16ZDA001N, which is part of the "Habitable Worlds" program, by the National Science Foundation under Award Nos. 1401554 and 1753373, by a University of California President's Postdoctoral Fellowship, and a Clare Boothe Luce Professorship. We would like to acknowledge high-performance computing support from Yellowstone (ark:/85065/d7wd3xhc) and Cheyenne (doi:10.5065/D6RX99HX) provided by NCAR's Computational and Information Systems Laboratory, sponsored by the National Science Foundation. A.S. thanks Cecilia Bitz for important discussions and generous help with code modification, Eric Wolf for providing useful code, and John Armstrong, Eric Agol, Shawn Domagal-Goldman, Raymond Pierrehumbert, and Jonathan Mitchell for helpful discussions. A.S. also thanks the Astrobiology Program and the Virtual Planetary Laboratory at the University of Washington for encouraging the types of interdisciplinary collaborations that resulted in this paper. We also thank an anonymous reviewer for beneficial feedback that greatly improved the paper.

# **ORCID iDs**

Aomawa L. Shields https://orcid.org/0000-0002-7086-9516

#### References

```
Abbot, D. S. 2016, ApJ, 827, 117
Abbot, D. S., Eisenman, I., & Pierrehumbert, R. T. 2010, JCli, 23, 6100
Abe, Y., Abe-Ouchi, A., Sleep, N. H., & Zahnle, K. J. 2011, AsBio, 11, 443
Anglada-Escudé, G., Amado, P. J., Barnes, J., et al. 2016, Natur, 536, 437
Bitz, C. M., Holland, M. M., Weaver, A. J., & Eby, M. 2001, JGRC, 106, 2441
Bitz, C. M., Shell, K. M., Gent, P. R., et al. 2012, JCli, 25, 3053
Bolmont, E., Selsis, F., Owen, J. E., et al. 2017, MNRAS, 464, 3728
Brandt, R. E., Warren, S. G., Worby, A. P., & Grenfell, T. C. 2005, JCli, 18, 3606
Carns, R. C., Brandt, R. E., & Warren, S. G. 2015, JGRC, 120, 7400
Carns, R. C., Light, B., & Warren, S. G. 2016, JGRC, 121, 5217
Chance, K., & Kurucz, R. L. 2010, JOSRT, 111, 1289
Checlair, J., Menou, K., & Abbot, D. S. 2017, ApJ, 845, 132
Dittmann, J. A., Irwin, J. M., Charbonneau, D., et al. 2017, Natur, 544, 333
Dobrovolskis, A. R. 2009, Icar, 204, 1
Dole, S. H. 1964, Habitable Planets for Man (New York: Blaisdell)
Edson, A., Lee, S., Bannon, P., Kasting, J. F., & Pollard, D. 2011, Icar, 212, 1
Gardner, J. P., Mather, J. C., Clampin, M., et al. 2006, SSRv, 123, 485
Gent, P. R., Danabasoglu, G., Donner, L. J., et al. 2011, JCli, 24, 4973
Gillon, M., Triaud, A. H. M. J., Demory, B.-O., et al. 2017, Natur, 542, 456
Haqq-Misra, J., Kopparapu, R. K., Batalha, N. E., Harman, C. E., &
   Kasting, J. F. 2016, ApJ, 827, 120
Hudson, S. R., Warren, S. G., Brandt, R. E., Grenfell, T. C., & Six, D. 2006,
   JGRD, 111, D181066
Hunke, E. C., & Lipscomb, W. H. 2008, CICE: The Los Alamos Sea Ice Model.
  Documentation and Software User's Manual. Version 4.0. (T-3 Fluid Dynamics
  Group, Los Alamos National Laboratory, Tech. Rep. LA-CC-06-012 )
Joshi, M. M., & Haberle, R. M. 2012, AsBio, 12, 3
Joshi, M. M., Haberle, R. M., & Reynolds, R. T. 1997, Icar, 129, 450
Kalirai, J. 2018, ConP, 59, 251
Kasting, J. F., Whitmire, D. P., & Reynolds, R. T. 1993, Icar, 101, 108
Kirschvink, J. 1992, in Late Proterozoic Low-Latitude Global Glaciation: The
  Snowball Earth, Vol. The Proterozoic Biosphere: A Multidisciplinary
  Study, ed. J. Schopf (Cambridge: Cambridge Univ. Press), 51
Leconte, J., Wu, H., Menou, K., & Murray, N. 2015, Sci, 347, 632
```

```
Light, B., Brandt, R. E., & Warren, S. G. 2009, JGRC, 114, C07018
Light, B., Carns, R. C., & Warren, S. G. 2016, JGRC, 121, 4966
Luger, R., & Barnes, R. 2015, AsBio, 15, 119
Menou, K. 2015, E&PSL, 429, 20
Pierrehumbert, R. 2005, JGRD, 110, D01111
Quintana, E. V., Barclay, T., Raymond, S. N., et al. 2014, Sci, 344, 277
Raymond, S. N., Scalo, J., & Meadows, V. S. 2007, ApJ, 669, 606
Reid, I. N., Hawley, S. L., & Gizis, J. E. 1995, AJ, 110, 1838
Ricker, G. R., Winn, J. N., Vanderspek, R., et al. 2014, Proc. SPIE, 9143, 914320
Seager, S. 2013, Sci, 340, 577
```

```
Segura, A., Kasting, J. F., Meadows, V., et al. 2005, AsBio, 5, 706
Shields, A. L., Ballard, S., & Johnson, J. A. 2016a, PhR, 663, 1
Shields, A. L., Barnes, R., Agol, E., et al. 2016b, AsBio, 16, 443
Shields, A. L., Bitz, C. M., Meadows, V. S., Joshi, M. M., & Robinson, T. D. 2014, ApJL, 785, L9
Shields, A. L., Meadows, V. S., Bitz, C. M., et al. 2013, AsBio, 13, 715
Walker, J. C. G., Hays, P. B., & Kasting, J. F. 1981, JGR, 86, 9776
Wolf, E. T., Shields, A. L., Kopparapu, R. K., Haqq-Misra, J., & Toon, O. B. 2017, ApJ, 837, 107
Yang, J., Boué, G., Fabrycky, D. C., & Abbot, D. S. 2014, ApJL, 787, L2
```